Accepted to the Astronomical Journal

Compact Symmetric Objects as Radio Flux Density Calibrators

C. D. Fassnacht[1] and G. B. Taylor

National Radio Astronomy Observatory

P. O. Box O, Socorro, NM 87801

cdf@stsci.edu, gtaylor@nrao.edu

ABSTRACT

We present results from the first intensive monitoring campaign of a sample of Compact Symmetric Objects (CSOs). We observed seven CSOs at 8.5 GHz over a period of eight months, with an average spacing between observations of 2.7 days. Our results show that, as predicted, the flux densities of the CSOs are extremely stable; the mean RMS variability of the sample was 0.7% in flux density. The low variability of the CSOs makes them excellent flux density calibrators at this frequency. We recommend that at least four CSOs be included in any VLA monitoring campaign which requires precise epoch-to-epoch calibration, such as those to measure gravitational lens time delays. The CSO data enable the correction of small systematic errors in the primary flux calibration.

Subject headings: galaxies: individual (]J1035+5628,]J1148+5924,]J1244+4048,]J1400+6210,]J1545+4751,]J1823+7938,]J1945+7055) — radio continuum — techniques: photometric

[1]Current Address: Space Telescope Science Institute 3700 San Martin Drive Baltimore, MD 21218

1. Introduction

For calibration of interferometric observations, it is generally desirable to employ unresolved calibrator sources. These sources have the advantage of appearing the same to all antenna pairs (visibilities), regardless of baseline length or orientation. Ideally, one would also prefer the flux density of the calibrators to be constant in time in order to facilitate removal of systematic atmospheric or instrumental variations. Calibrators that are unpolarized have added benefits in solving for the instrumental polarization terms.

Unfortunately (from the perspective of calibration) most compact (size $< 0\farcs1$) extragalactic radio sources are highly variable. These sources, which have flat radio spectra, have flux densities that vary by $\sim$10% on timescales of weeks to months and can easily vary by $\sim$100% on timescales of months to years (Aller, Hughes, & Aller 1990). Quirrenbach et al. (1992) found low-amplitude (1–2%) intra-day variability in all flat-spectrum sources, and larger variations (up to 20%) in $\sim$25% of these sources. VLBI imaging of a large flux-limited sample (Taylor et al. 1996b) reveals that 95% of compact, flat-spectrum sources have asymmetric, core-jet morphologies. The core is generally the dominant component and has a typical size of less than 0.1 mas (under a parsec for typical redshifts). The variability can thus be explained by the short light-crossing time of the emitting volume, and/or refractive interstellar scintillation in the Galactic ISM. The jet components exhibit superluminal motions and are probably moving at relativistic speeds (Vermeulen & Cohen 1994). Flares in the jet components have also been observed with similar amplitudes and timescales as core flares (Zhou et al. 2000).

There is, however, a small fraction (5%; Peck & Taylor 2000) of compact sources whose pc-scale structure is dominated by steep-spectrum extended emission on both sides of the core. These sources are known as Compact Symmetric Objects (CSOs). Recent measurements of kinematic ages of $\sim$1000 years (Owsianik & Conway 1998; Owsianik, Conway, & Polatidis 1998; Taylor et al. 2000) support the theory that CSOs are small by virtue of their youth and not because they are frustrated by a dense environment. This was the favored interpretation by Phillips & Mutel (1980, 1982) who first drew attention to a group of compact double sources with steep or GHz-peaked spectra and slow motions compared to the majority of core-jet sources. At about the same time, Rudnick & Jones (1982) reported that GHz-peaked spectrum (GPS) sources generally have low variability and low polarization. Although there is some overlap between sources classified as CSOs and those classified as GPS sources, we emphasize that there is no clear correspondence between the two types of sources. In fact, a recent survey of 47 GPS sources found that only 3 could be clearly classified as CSOs (Snellen, Schilizzi, & van Langevelde 2000). The term GPS is purely a spectral classification while CSO is a physical one, requiring considerably greater observational effort (usually VLBI observations at multiple frequencies) in order to identify the location of the core component and extended jet and/or lobe emission on both sides of the core. Objects with vastly different powers, orientations, and evolutionary stages can be classified as GPS sources, while the CSOs are a much more homogeneous group. The lack of correspondence between GPS and CSO sources is especially important to keep in mind if one is choosing a sample of CSOs as flux density calibrators.

The CSOs have qualities which should make them excellent flux calibrator sources. One is the relative unimportance of the presumably variable core component. For 6 bright CSOs, Taylor, Readhead, & Pearson (1996a) found the core to comprise from <0.4% to 6% of the integrated flux density at 15 GHz. Another quality is that the jets and lobes of CSOs are thought to be relatively free of Doppler boosting effects (Wilkinson et al. 1994). Thus, flux variations due to flares in the jet components should not be magnified. The physical properties of CSOs have been summarized by Readhead et al. (1996), who pointed out that the few CSOs known at that time exhibited both weak radio variability ($< 10\%$) and low polarization ($< 0.5\%$). In addition, de Bruyn (1991) reported that the CSO OQ 208 (classification based on the VLBI images by Stanghellini et al. 1997) varied by less than 2% yr^{-1} over a period of 10 years at 5 GHz. Peck & Taylor (2000) presented 8.4 GHz VLBI observations showing that the polarization was less than 1% in 21 CSOs and CSO candidates. Yet another fortunate property of CSOs for calibration purposes is that they generally exhibit no emission on scales greater than 1 kpc. An exception to this rule is the CSO 0108+388 which has some faint extended emission (Baum et al. 1990). Another exceptional source is the CSO J1148+5924 (NGC 3894) which also has faint kpc-scale emission and has been seen to be slowly variable on timescales of years (Taylor, Wrobel, & Vermeulen 1998). J1148+5924 is relatively nearby at a redshift of 0.01085 (van Gorkom et al. 1989), and has a luminosity more than two orders of magnitude less than all other members of the CSO class.

In §2 we present observations of seven CSOs used as calibrators in an intensive VLA monitoring campaign. The calibration procedure is described in §3. In §4 and §5 we consider primary and secondary systematic errors which allows us to provide, in §6, a prescription for obtaining high-precision monitoring. Lastly, in §7 we consider how variability studies can be used to constrain physical models for CSOs.

2. Observations

The sample observed for this paper consisted of seven CSOs chosen from the samples of Peck & Taylor (2000) and Taylor et al. (1996b). These particular sources were observed as part of a gravitational lens monitoring campaign and were chosen because they were bright and were located in the RA range defined by the lens systems. The sources and their coordinates are listed in Table 1. The observations were made with the VLA[2] at 8.5 GHz during its A, BnA, and B configurations, yielding typical angular resolutions of $0\farcs2$ in the A configuration to $0\farcs7$ in the B configuration. The monitoring program consisted of 88 observations of the sample between 1999 June 21 and 2000 February 14, giving an average spacing of 2.7 d between epochs. The typical observing block was one or two hours in length, and the typical integration time on each of the CSOs was 45 or 60 sec. For each epoch, some fraction of the CSO sample was observed at a large hour angle, since the CSOs are widely spaced on the sky and the observing blocks were short. In fact, it was not always possible to observe the entire sample of CSOs in an observing block. However, the incomplete sampling should not significantly affect the conclusions of this paper. All of the CSOs were observed at least 68 times, giving quite adequate determinations of their light curves.

In addition to the CSOs and the lens systems, two phase calibrators were observed as part of the monitoring program (Table 2). The typical integration times on the phase calibrators were between 2 and 3 min. These two sources will also be discussed in this paper because they provide a useful contrast to the CSO sample. The lenses will be discussed in a series of future papers. All of the sources discussed in this paper can be found in the list of VLA calibrators maintained by NRAO[3].

3. Calibration and Data Reduction

The data were calibrated in the AIPS software package developed by NRAO. The standard flux density calibrator 3C 286 was not observed for all epochs, so the overall flux density calibration was instead tied to the source 3C 343 (1634+628). This source has a steep two-point radio spectral index between 1.4 and 8.5 GHz ($\alpha \sim -1.0$; $S_\nu \propto \nu^\alpha$) and its flux density has been shown to be stable in past monitoring campaigns (Fassnacht et al. 1999). Although the emission from 3C 343 is dominated by the compact central component, there is some low surface-brightness extended emission from the source. Because of the extended emission, 3C 343 is not an ideal flux calibrator. First, the total flux density measured for the source will change with the VLA configuration, since the more compact configurations are more sensitive to the low surface-brightness emission. To correct for this effect, we scaled the 3C 343 flux densities by factors of 0.997 and 0.983 for the BnA and B configurations,

[2]The National Radio Astronomy Observatory is operated by Associated Universities, Inc., under cooperative agreement with the National Science Foundation.

[3]http://info.aoc.nrao.edu/~gtaylor/calib.html

Table 1. CSO Sample

Name (B1950)	Name (J2000)	RA(2000)	Dec(2000)
1031+567	J1035+5628	$10^{h}35^{m}07\overset{s}{.}040$	$+56^{\circ}28'46\overset{''}{.}79$
1146+596	J1148+5924	$11^{h}48^{m}50\overset{s}{.}358$	$+59^{\circ}24'56\overset{''}{.}38$
1242+410	J1244+4048	$12^{h}44^{m}49\overset{s}{.}196$	$+40^{\circ}48'06\overset{''}{.}22$
1358+624	J1400+6210	$14^{h}00^{m}28\overset{s}{.}653$	$+62^{\circ}10'38\overset{''}{.}53$
1543+480	J1545+4751	$15^{h}45^{m}08\overset{s}{.}530$	$+47^{\circ}51'54\overset{''}{.}67$
1826+796	J1823+7938	$18^{h}23^{m}14\overset{s}{.}109$	$+79^{\circ}38'49\overset{''}{.}00$
1946+708	J1945+7055	$19^{h}45^{m}53\overset{s}{.}520$	$+70^{\circ}55'48\overset{''}{.}72$

Table 2. Phase Calibrators (Core-Jet Sources)

Name (B1950)	Name (J2000)	RA(2000)	Dec(2000)
1547+507	J1549+5038	$15^{h}49^{m}17\overset{s}{.}469$	$+50^{\circ}38'05\overset{''}{.}79$
1642+690	J1642+6856	$16^{h}42^{m}07\overset{s}{.}849$	$+68^{\circ}56'39\overset{''}{.}76$

respectively. Secondly, the changing (u, v) coverage for each monitoring epoch may cause small variations in the measured flux density since different (u, v) coverages are sensitive to different source structures. However, these small variations, as well as those caused by the changing observing conditions and any intrinsic variability in 3C 343, can easily be corrected for, as shown in §4.

Because the CSOs in our sample are compact and bright ($S_{8.5} > 200$ mJy; Table 3), they can be used to determine antenna gain solutions without the need for an external calibrator. For two of the sources, J1035+5628 and J1400+6210, the emission from the source is slightly resolved. Thus, for these two CSOs, the gain solutions were calculated only for baseline lengths that were less than 400 kλ. For all of the other CSOs, all baselines were used. For each CSO, two iterations of the AIPS task CALIB were run. In the first, only the gain phases were solved for, with a solution interval of 10 sec. The phase solutions were applied to the data and then the second iteration of CALIB was performed. In this iteration, both amplitude and phase solutions were obtained, with a solution interval of 30 sec. The phase calibrators were processed in the same manner.

After the data were calibrated, we measured the CSO flux densities using two separate methods. The first method was to use the GETJY task within AIPS, which computes the flux density based on the gain solutions calculated in CALIB. The second method was to export the files from AIPS and to fit models to the (u, v) data using the `difmap` package (Shepherd 1997). The `difmap` processing is more flexible in dealing with source structure than the GETJY task. However, since the emission from CSOs is dominated by an unresolved or barely resolved component, the two methods should not greatly differ in the results that they produce. This is, in fact what we see. We compared the GETJY and `difmap` flux densities for all the CSOs and found that the mean difference in flux density is $0.07\% \pm 0.18\%$. The results presented in this paper are for the `difmap` flux densities. However, we have also analyzed the data obtained from the GETJY step and find no significant difference in the results.

4. Correction for Primary Systematic Errors

To compare the variability of the CSOs in our sample, we normalized the light curves of each CSO by the mean flux density, $< S_i >$, recorded for that CSO over the course of the monitoring program. The values of N_i, the number of observations obtained on source i, and $< S_i >$ are recorded in Table 3. We then defined the normalized light curves, $S^N_{i,j}$, as as

$$S^N_{i,j} = \frac{S_{i,j}}{< S_i >}, \qquad i = 1035, 1148, 1244, 1400, 1545, 1823, 1945$$

where $S_{i,j}$ is the flux density of source i on day j. The normalized light curves of the seven CSOs are shown in Figure 1. The S^N curves show considerable scatter about the mean value of 1.0, up to nearly 10% for some days, and the RMS scatter about the mean for the entire sample is 1.3%. This is a little better than the canonical absolute accuracy of 2% quoted for standard VLA observations. However, a significant portion of the scatter is due to systematic rather than random errors. Although it may not be immediately obvious from the plot, the CSO light curves track each other in the sense that on certain days all of the measured flux densities will be above the mean and on other days all will be below the mean. This behavior results from small errors in the absolute flux density calibration derived from 3C 343, which are due to a combination of errors in the AIPS calibration process (see §3) and the possible small intrinsic variability of the calibrator. The same effect is seen, perhaps more clearly, in the steep-spectrum source light curves shown in Fassnacht et al. (1999), for which the absolute flux density calibration was derived from 3C 286. We have to remove the calibration errors in order to evaluate properly the variability of the CSO sample.

Fortunately, the data themselves contain the information necessary to correct for the systematic errors in the flux density calibration. We assume that any intrinsic variability in our sample of CSOs is not correlated from source to source. Thus, any correlated variations in the light curves, such as the large variations seen on days 1481 and 1523.5 in Figure 1, must be due to systematic errors in the absolute flux density calibration. To correct for the flux calibration errors, we construct a light curve, $M^{(1)}$, that represents our estimate of the effect of those errors. This curve is simply the median of the normalized CSO flux densities recorded for each epoch, i.e.,

$$M_j^{(1)} = \mathrm{median}(S_{i,j}^N).$$

The resulting $M^{(1)}$ curve is represented by the dark line in Figure 1. We then divide the CSO light curves by the median curve to perform the correction. The median-corrected light curves,

$$S_{i,j}^M = \frac{S^N i, j}{M_j^{(1)}},$$

are shown in Figure 2. The variability in the corrected light curves is now due to small, uncorrelated variations about their mean values. The RMS offsets from the mean are given in the "$M^{(1)}$ RMS" column of Table 3. The total RMS of the sample as a whole is 0.99%.

5. Secondary Systematic Errors

Table 3 shows that the sources J1823+7938 and J1945+7055 have nearly double the RMS scatter of the other CSOs in the sample. This can also be seen in the plot in Figure 2

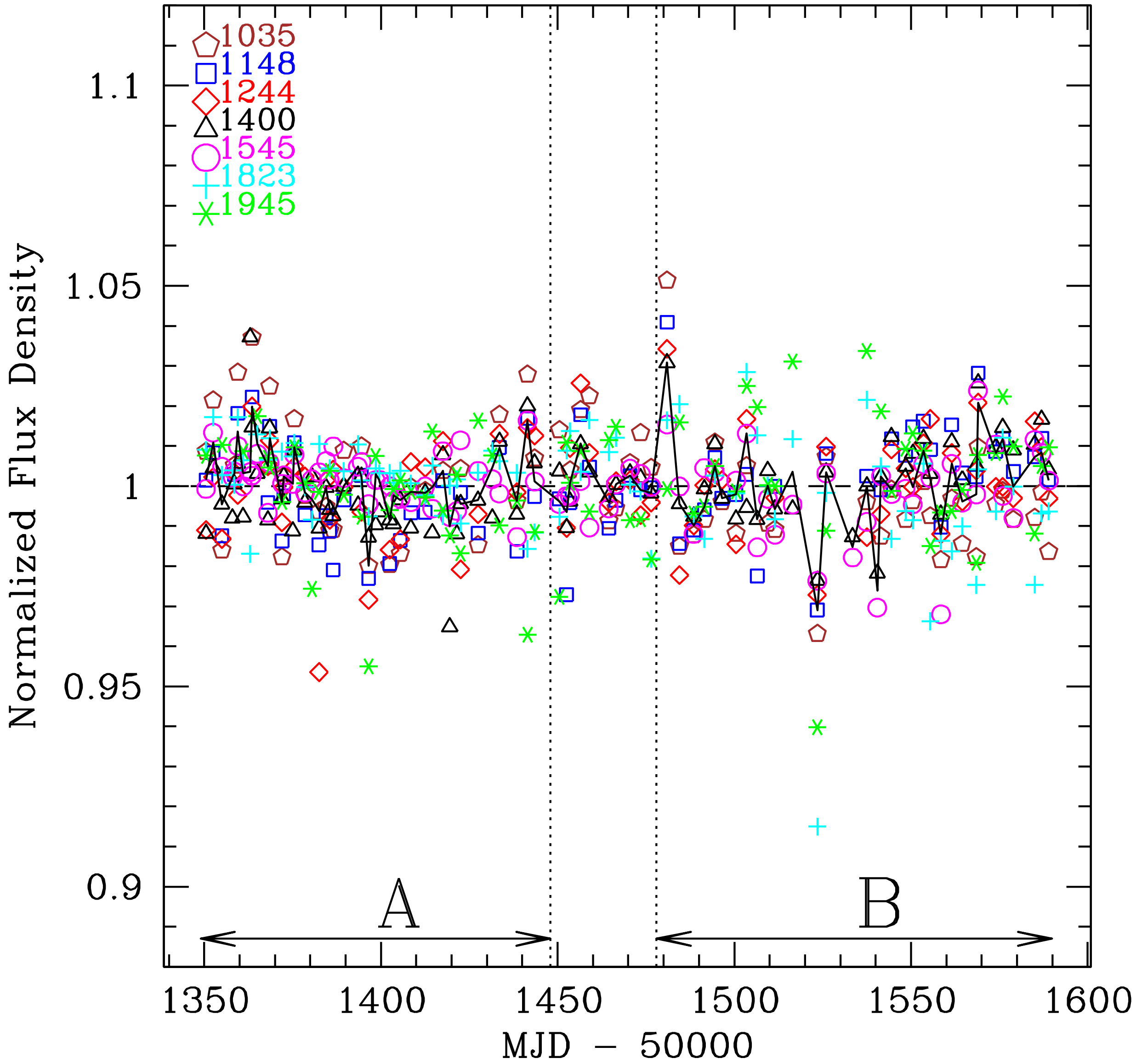

Fig. 1.— Normalized light curves of the seven CSO sources. The abscissa is time, with units of MJD - 50000. The ordinate is normalized flux density, so the plotted points represent fractional deviations from the mean. The heavy black line indicates the median normalized flux density, $M^{(1)}$, for each day of observation. The vertical dotted lines delineate the VLA configuration. The A and B configurations are labeled. The unlabeled configuration is the BnA configuration. For clarity, the error bars on the points are not shown. The formal errors, estimated from the RMS noise in the residual maps, are approximately the size of the points in the plot.

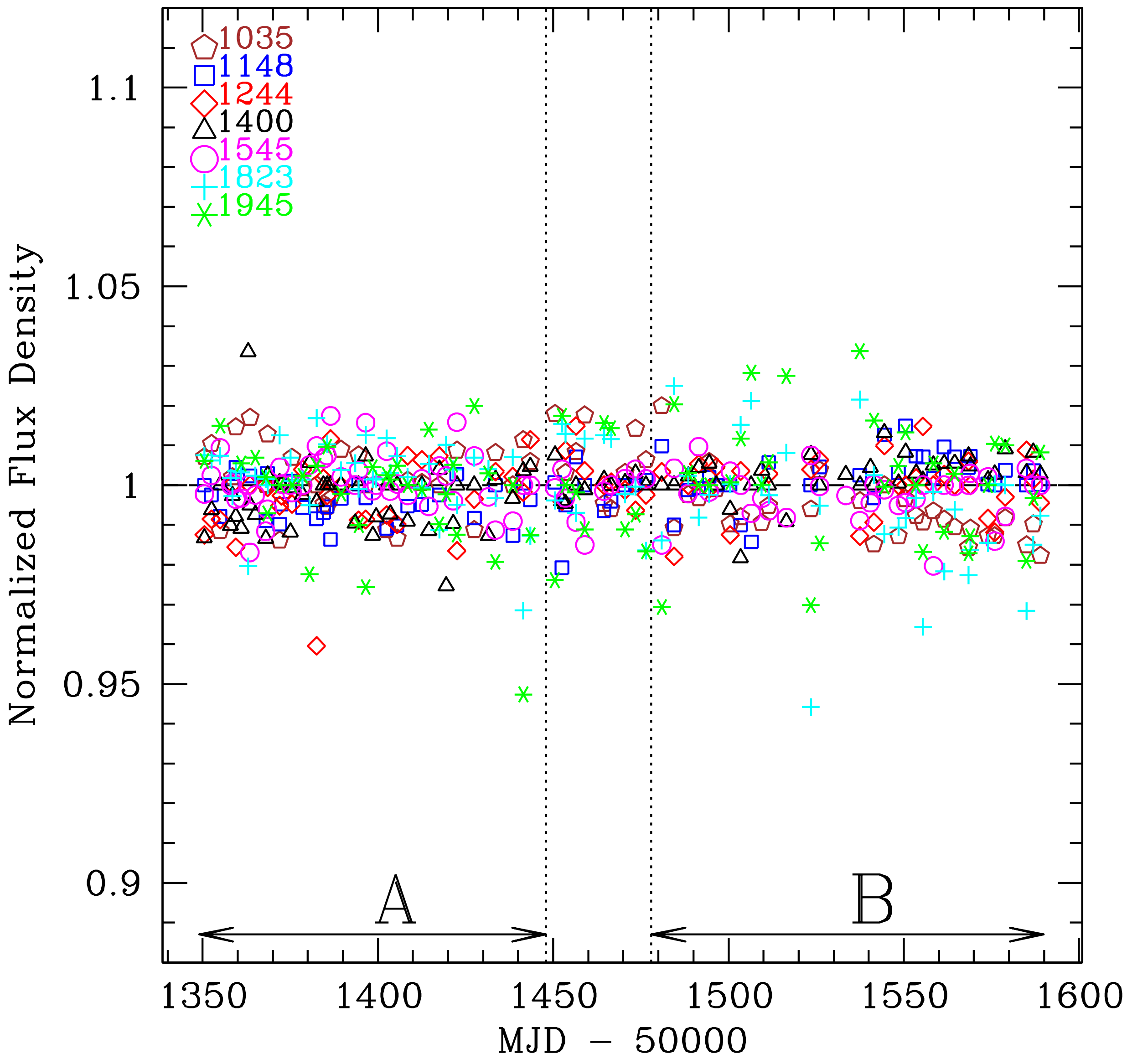

Fig. 2.— Same as Figure 1 except all light curves have been divided by the median curve, $M^{(1)}$, to account for errors in the flux density calibration.

where the J1823+7938 (+) and J1945+7055 (*) points are clearly visible above the sample scatter, especially in the B-configuration data. On the face of it, these variations are small and would not be a cause for worry. However, upon closer examination of the light curves, it becomes apparent that there is an additional systematic error affecting the light curves of these two sources. The presence of the additional error is also clearly evident when we calculate the linear correlation coefficient (e.g., Bevington 1969) between all the possible pairs of the CSO light curves. We show the effect of this error in Figure 3, in which only the light curves of J1823+7938 and J1945+7055, i.e., S^M_{1823} and S^M_{1945}, are plotted. Not only do the light curves show a larger scatter than the other CSO curves, but the deviations from the mean appear to be correlated. The light curves track each other very closely, especially in the large variations seen in the B-configuration data. We have not been able to determine the cause of this secondary systematic error. For example, the flux densities measured for these two sources are not correlated with either the elevation of the CSO at the time of observation, or the difference in elevation between the flux calibrator (3C 343) and the CSO. We do note that these CSOs are the two most northern in the sample, both with $\delta > 70°$, but we do not know of any property of the VLA that would only affect far northern sources. We have considered the possibility that this error could be due to a systematic problem with the pointing model, but we have found no other evidence in the long history of VLA pointing runs to support this conclusion. Because we cannot determine the source of this systematic effect, we do not correct for it. As a result, the RMS variations listed in Table 3 for these two sources should be regarded as upper limits to their true intrinsic level of variability. For the remainder of our discussion of the CSO sample we will discard J1823+7938 and J1945+7055.

Although it is unlikely that systematic errors with the pointing models can account for the correlated behavior of the light curves for J1823+7938 and J1945+7055, it may be that small pointing errors are introducing some of the scatter observed in the CSO light curves. It is possible to calculate corrections to the VLA antenna pointing models through specialized observations of strong compact sources prior to observing the sources of interest. However, these corrections need to be re-calculated each time the antennas make a significant move. Due to the wide spacing of our CSO sample on the sky and the short observing blocks, we did not have sufficient time to make the additional observations necessary to calculate these corrections. Future programs to study CSO variability should strongly consider allocating time in their programs specifically for determining the pointing solution corrections. It should be possible to use observations of the CSOs themselves to determine the corrections.

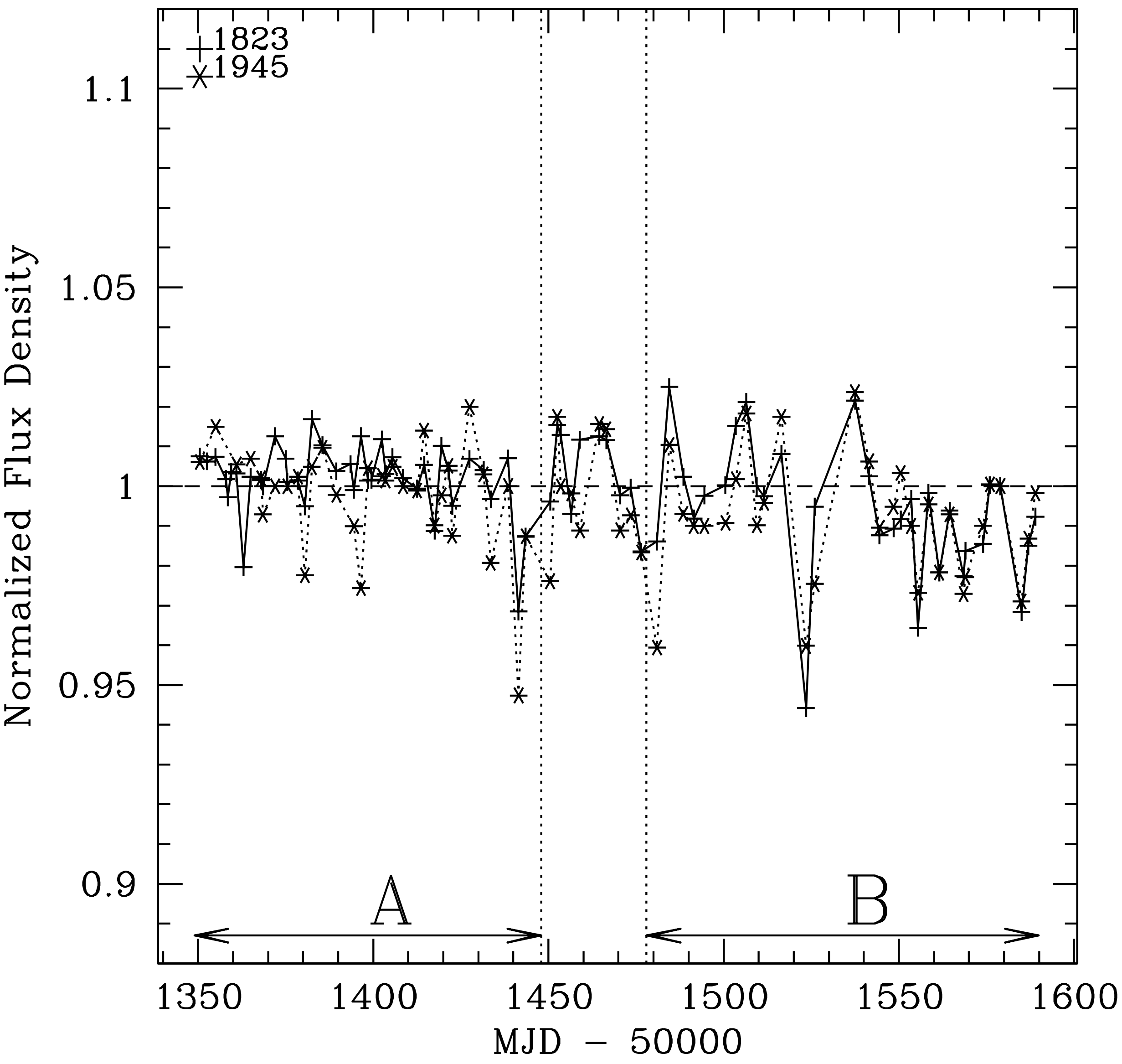

Fig. 3.— Same as Figure 2 except that only the light curves for the sources J1823+7938 and J1945+7055 are shown. The variations in the two light curves appear correlated from day 1405 onward, and are especially well-matched from day 1540 onward. To emphasize the similarity of the day-to-day variations, the B-configuration light curve for J1945+7055 has been shifted downward by 0.01.

6. Final Light Curves and a Prescription for High-Precision Radio Monitoring

To create the final CSO light curves, we discarded the data from J1823+7938 and J1945+7055 and then used the light curves of the remaining five CSOs to create a new correction curve, $M^{(2)}$. Because the sources contributing the bulk of the outlier points had been discarded, we created the $M^{(2)}$ curve from the mean of the normalized light curves rather than their median, i.e.,

$$M_j^{(2)} = \frac{\sum_i (S_{i,j}^N)}{N_j}, \qquad i = 1035, 1148, 1244, 1400, 1545$$

where N_j is the number of CSOs that were observed on day j. The final corrected light curves,

$$S_{i,j}^{\rm final} = \frac{S_{i,j}^N}{M_j^{(2)}}$$

are shown in Figure 4.

It is now possible to estimate the intrinsic variability of the CSOs from the final light curves. In principle, the RMS scatter of the $S^{\rm final}$ curves gives an estimate of the variability of the sources. However, it is important to realize that the division of the input S^N curves by the $M^{(2)}$ light curve is an operation on two correlated quantities. That is, each point in the S^N curves gets scaled by a quantity that includes a contribution from itself. As a result, the division by the $M^{(2)}$ curve has the effect, on average, of depressing the measured RMS of the $S^{\rm final}$ curves below their true intrinsic scatter. We have estimated the correction for this effect, in a statistical sense, by using the measured RMS scatter in the $S^{\rm final}$ curves. The measured and corrected RMS scatters for each source are given in the "$M^{(2)}$ RMS" and "Intrinsic RMS" columns of Table 3, respectively. The maximum correction is only $\Delta\,$RMS=+0.15% and, thus, our conclusion that the CSOs have extremely stable flux densities does not change. Whether we use the "$M^{(2)}$" or "Intrinsic" values for the RMS variability of the CSOs, we find that the mean RMS scatter for the five CSOs is $\sim$0.7%. This is the same value obtained by considering the combined sample of CSOs to be one distribution and calculating its RMS scatter about the mean. Finally, we note that the estimated intrinsic variabilities that we have derived above may still include unknown systematic errors and thus should be regarded as upper limits.

The CSO light curves can be contrasted with those of the phase calibrators, both of which are core-jet sources on the parsec scale (Fey & Charlot 1997), shown in Figure 5. The core-jet light curves have been processed in the same manner as the CSO light curves, including the correction with the $M^{(2)}$ curve. Not only do the core-jet calibrator curves have

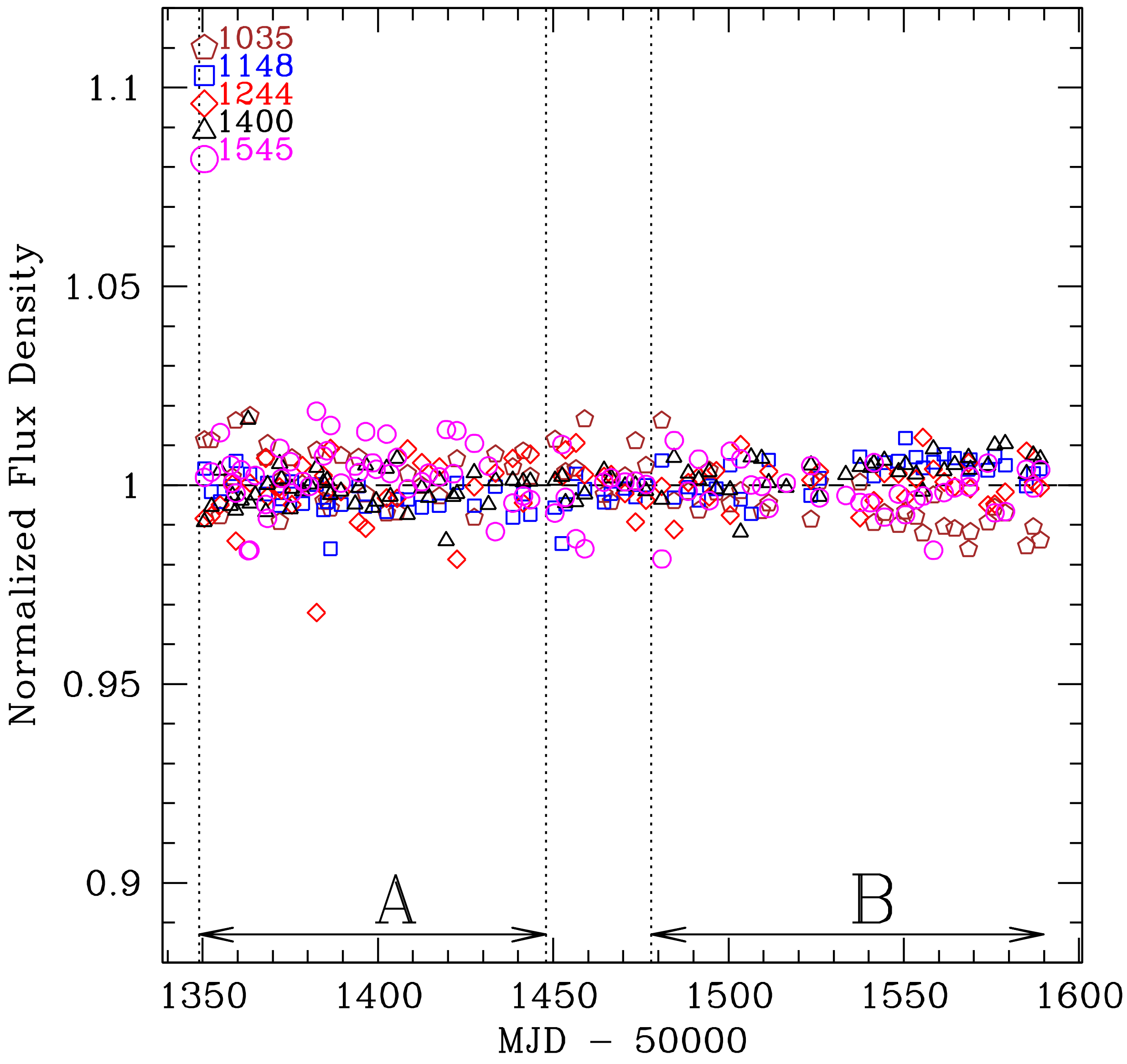

Fig. 4.— Final CSO light curves. The light curves have been divided by the $M^{(2)}$ curve, which was constructed by excluding the data from J1823+7938 and J1945+7055.

a higher RMS scatter than do the CSO light curves (Table 4), but the nature of the core-jet light curves is qualitatively different from those of the CSOs. Instead of random scatter about the mean value, the core-jet sources show systematic changes in flux density during the course of the observations, indicating true variability at the level of nearly 10%. They also exhibit variability from 2–5% from epoch to epoch.

Given the nature of the CSO light curves, which show only small and random variations about a mean value, we conclude that the CSO sources should make excellent flux density calibrators for radio monitoring campaigns. If high-precision relative calibration is desired, we recommend that at least four CSOs be observed in each epoch, if possible. With this observing strategy, it should be possible to account correctly for systematic errors in the overall flux density calibration. In addition, having at least four CSO calibrators enables the rejection of any one of the calibrators if something adversely affects its measured flux density, for either the entire monitoring campaign or a single epoch. We emphasize, again, that CSOs should not be equated with GPS sources, especially for the purpose of flux density calibration.

7. Physical Constraints on CSOs from Variability

The average variability for five CSOs is 0.7%, excluding the two high-declination sources J1823+7938 and J1945+7055. This average value doubtless includes some, as yet poorly understood, residual systematic errors. Until such a time as we can demonstrate reproducible flux density measurement with less scatter, this value should be considered an upper limit on the true variability of CSOs. Even so we can use this limit to estimate the fraction of the luminosity coming from a compact core, and eventually to constrain the evolution of CSOs.

The total variability of core-jet sources is typically $\sim$3% (Quirrenbach et al. 1992, also see Figure 5). Taking an average core fraction of 0.6 from VLBI observations (Taylor et al. 1996b), we can estimate the real variability of the core components to be $\sim$5%. If the core components in CSOs behave similarly then we could use the observed variability of 0.7% to estimate that the core fraction in CSOs to be $\sim$0.14. In fact a more typical estimate from VLBI images is 0.03 (Taylor et al. 1996a). Both the CSO variability and the typical core fraction are derived from small samples with only one source in common (J1400+6210). However, assuming that they are still indicative of the average properties we can conclude that the core components in CSOs are a factor 5 less variable than cores in core-jet sources. This could indicate that the less-beamed cores are physically larger in CSOs and therefore much less affected by refractive interstellar scattering in the ISM.

Table 3. CSO Variability

Source	N_i	$< S_i >$ (mJy)	$M^{(1)}$ RMS (%)	$M^{(2)}$ RMS (%)	Intrinsic RMS (%)
J1035+5628	69	768	0.95	0.83	0.98
J1148+5924	70	436	0.66	0.53	0.53
J1244+4048	68	438	0.87	0.72	0.82
J1400+6210	88	1108	0.75	0.50	0.48
J1545+4751	87	323	0.67	0.75	0.86
J1823+7938	81	537	1.3	⋯	⋯
J1945+7055	73	441	1.5	⋯	⋯

Table 4. Core-Jet Variability

Source	N_i	$< S_i >$ (mJy)	$M^{(2)}$ RMS (%)
J1549+5038	86	921	3.0
J1642+6856	88	859	2.9

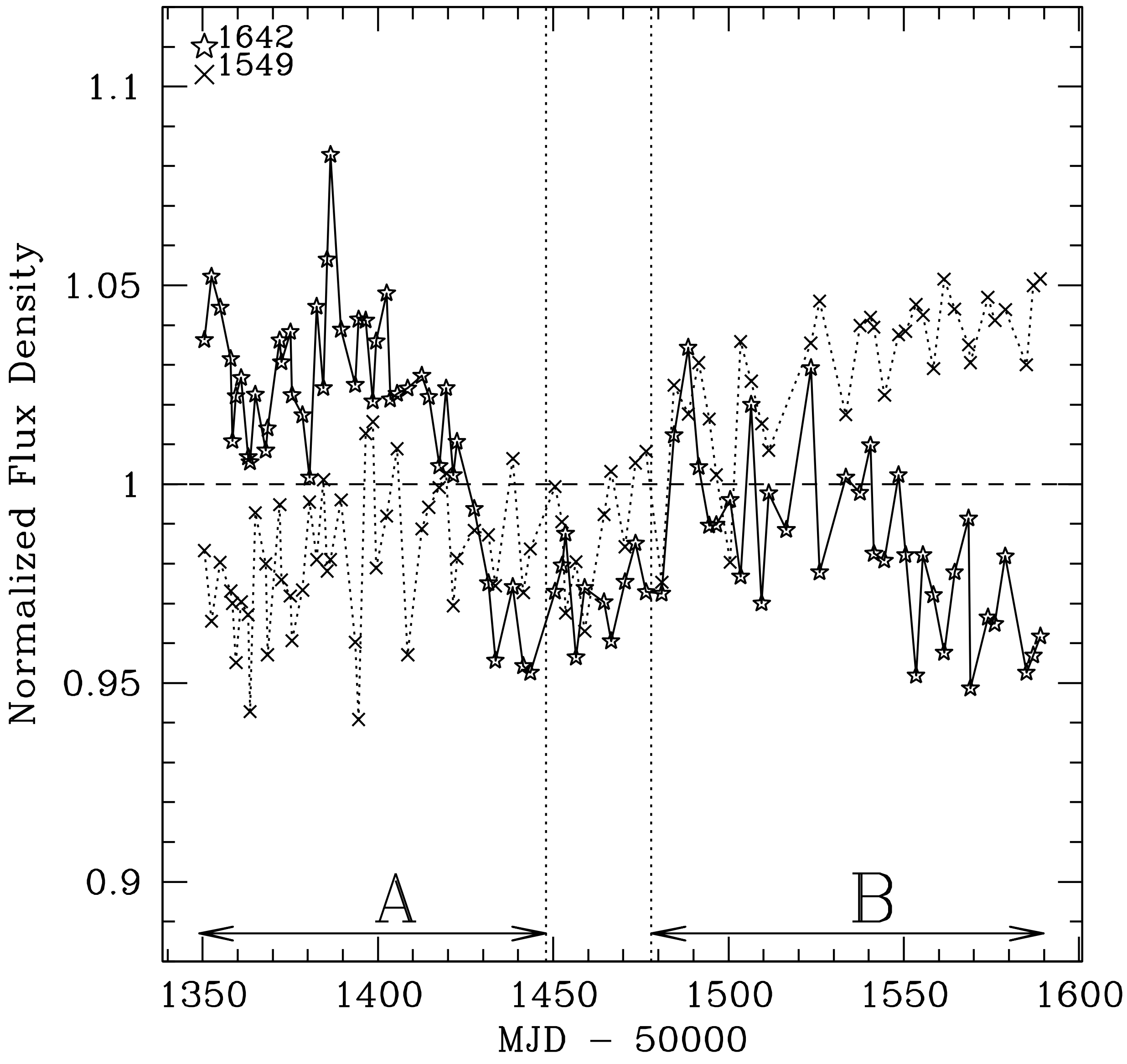

Fig. 5.— Final light curves for the two core-jet sources. These light curves have been normalized by their mean flux density and then divided by the $M^{(2)}$ curve. Note that both sources undergo systematic changes in flux density with time, at a level of a few percent.

Readhead et al. (1996) derive empirical relationships for the evolution of of powerful radio galaxies from the CSO phase into classical double radio galaxies like Cygnus A. They find evidence for a modest decrease in luminosity, L, as the radio source grows in size, r, according to $L \propto r^q$ where $q = -0.35$. Current estimates of the hot spot advance speed in CSOs is 0.1c (Owsianik & Conway 1998; Taylor et al. 2000). In 1 year a typical CSO, of size $\sim$100 ly, will grow by 0.2 ly, or 0.2%. The predicted change in luminosity is -0.07% yr^{-1}. Our current measurements range from -2.6 to 1.3% yr^{-1}, with an average value of -0.42% yr^{-1} and an RMS of 1.7% yr^{-1}. To provide an adequate test of the empirical relations proposed by Readhead et al. (1996) will require an order of magnitude improvement in the measured variations. Observations of the sort reported here, spread out over $\sim$200 days are unlikely to achieve this with currently available instruments. With fiber optic transmission, a new correlator, and additional antennas in the southwest, the Expanded VLA (EVLA) should have both increased stability and the capability of using a subarray comprised of antennas in the southwest US to monitor gravitational lenses and CSOs with high resolution for the $\sim$3 years needed to achieve the desired accuracy.

8. Summary

We monitored a sample of seven CSOs with the VLA over the course of eight months. The flux densities of all of the sources were very stable, with only small measured variations about their mean value. We find that five of the CSOs have RMS variations of less than 1%. For these sources the average measured RMS is 0.7% and the RMS variability of the sample as a whole is also 0.7%. For the remaining two CSOs we estimate upper limits on the RMS variability of 1.5% or less. We conclude that CSOs, in general, are flux stable on time scales between 1 week and 10 months. Given this stability, they are excellent flux density calibrators for monitoring experiments. For a high precision experiment, we recommend that at least four of these CSOs be included in the observations.

For useful discussions, we thank Neal Miller, Stefano Casertano, Tim Pearson, Alison Peck, Lori Lubin, Steve Myers, Frazer Owen, Rick Perley, Adam Riess, and Ken Sowinski. We are grateful to Leon Koopmans, David Rusin, and Emily Xanthopoulos for help in choosing the CSO sample and in planning the observations. We thank the anonymous referee for suggestions that improved the paper. Meri Stanley, Jason Wurnig, and Ken Hartley did their usual excellent job in checking over the observing schedules and catching mistakes. We thank the NRAO staff for keeping the VLA running smoothly.

REFERENCES

Aller, H. D. Hughes, P. A., & Aller, M. F. 1990, in "Variability of Active Galactic Nuclei" eds. R. Miller & P. J. Wiita, (Cambridge Univ. Press:Cambridge), p. 172

Baum, S. A., O'Dea, C. P., de Bruyn, A. G., & Murphy, D. W. 1990, A&A, 232, 19

Bevington, P. R. 1969, *Data Reduction and Error Analysis for the Physical Sciences*, (New York: McGraw-Hill)

de Bruyn, A. G. 1991, in *Variability of Active Galaxies*, eds. W.J. Duschl, S.J. Wagner & M. Camenzind, (Springer–Verlag: New York) p. 105

Fassnacht, C. D., Pearson, T. J., Readhead, A. C. S., Browne, I. W. A., Koopmans, L. V. E., Myers, S. T., & Wilkinson, P. N. 1999, ApJ, 527, 498

Fey, A. L. & Charlot, P. 1997, ApJS, 111, 95

Owsianik, I. & Conway, J. E. 1998, A&A, 337, 69

Owsianik, I., Conway, J. E., & Polatidis, A. G. 1998, A&A, 336, L37

Peck, A. B. & Taylor, G. B. 2000, ApJ, 534, 90

Phillips, R. B. & Mutel, R. L. 1980, ApJ, 236, 89

Phillips, R. B. & Mutel, R. L. 1982, A&A, 106, 21

Quirrenbach, A. et al. 1992, A&A, 258, 279

Readhead, A. C. S., Taylor, G. B., Xu, W., Pearson, T. J., Wilkinson, P. N., & Polatidis, A. G. 1996, ApJ, 460, 612

Readhead, A. C. S., Taylor, G. B., Pearson, T. J., & Wilkinson, P. N. 1996, ApJ, 460, 634

Rudnick, L. & Jones, T. W. 1982, ApJ, 255, 39

Shepherd, M. C. 1997, in *Astronomical Data Analysis Software and Systems VI*, eds. G. Hunt & H. E. Payne, (ASP Conference Series, v125) 77

Snellen, I. A. G., Schilizzi, R. T., & van Langevelde, H. J. 2000, MNRAS, 319, 429

Stanghellini, C., Bondi, M., Dallacasa, D., O'Dea, C. P., Baum, S. A., Fanti, R., & Fanti, C. 1997, A&A, 318, 376

Taylor, G. B., Readhead, A. C. S., & Pearson, T. J. 1996a, ApJ, 463, 95

Taylor, G. B., Vermeulen, R. C., Readhead, A. C. S., Pearson, T. J., Henstock, D. R., & Wilkinson, P. N. 1996b, ApJS, 107, 37

Taylor, G. B., Wrobel, J. M., & Vermeulen, R. C. 1998, ApJ, 498, 619

Taylor, G. B., Marr, J. M., Pearson, T. J., & Readhead, A. C. S. 2000, ApJ, 541, 112

van Gorkom, J. H., Knapp, G. R., Ekers, R. D., Ekers, D. D., Laing, R. A., & Polk, K. S. 1989, AJ, 97, 708

Vermeulen, R. C. & Cohen, M. H. 1994, ApJ, 430, 467

Wilkinson, P. N., Polatidis, A. G., Readhead, A. C. S., Xu, W., & Pearson, T. J. 1994, ApJ, 432, L87

Zhou, J. F., Hong, X. Y., Jiang, D. R., & Venturi, T. 2000, ApJ, 541, L13
